

The Dynamical Kernel Scheduler - Part 1

Andreas Adelman^{a,*}, Uldis Locans^{a,b}, Andreas Suter^a

^aPaul Scherrer Institut, Villigen, CH-5232, Switzerland

^bUniversity of Latvia, 19 Raina Blvd., Riga, LV 1586, Latvia

Abstract

Emerging processor architectures such as GPUs and Intel MICs provide a huge performance potential for high performance computing. However developing software using these hardware accelerators introduces additional challenges for the developer such as exposing additional parallelism, dealing with different hardware designs and using multiple development frameworks in order to use devices from different vendors.

The Dynamic Kernel Scheduler (DKS) is being developed in order to provide a software layer between host application and different hardware accelerators. DKS handles the communication between the host and device, schedules task execution, and provides a library of built-in algorithms. Algorithms available in the DKS library will be written in CUDA, OpenCL and OpenMP. Depending on the available hardware, the DKS can select the appropriate implementation of the algorithm.

The first DKS version was created using CUDA for the Nvidia GPUs and OpenMP for Intel MIC. DKS was further integrated in OPAL (Object-oriented Parallel Accelerator Library) to speed up a parallel FFT based Poisson solver and Monte Carlo simulations for particle matter interaction used for proton therapy degrader modeling. DKS was also used together with Minuit2 for parameter fitting, where χ^2 and max-log-likelihood functions were offloaded to the hardware accelerator. The concepts of the DKS, first results together with plans for the future will be shown in this paper.

Keywords: GPGPU, CUDA, Intel MIC, FFT, Monte Carlo, OPAL, μ SR

*Corresponding author

Email address: andreas.adelmann@psi.ch (Andreas Adelman)

1. Introduction

Usage of hardware accelerators has become increasingly popular in scientific computing in recent years, based on the Top500 list from June 2015 [1], 90 of the top500 supercomputers in the world are accelerator based, including the top two systems on the list, Tianhe-2 which uses Intel Xeon Phi and Titan which uses NVIDIA K20x. GPU usage for general purpose computing has become even more important, because, thanks to the gaming industry, almost every computer is now equipped with a GPU and if the application is not exploiting the GPU it is not using all the available computational power of the system. However, developing software that can take advantage of hardware accelerators can become a challenging task, especially for large existing applications. Each hardware accelerator has its own architecture, its own memory hierarchy, and it is necessary to take all that into account to gain the maximum performance out of the device. In addition to hardware differences there are also different ways to program these devices. NVIDIA provides the CUDA [2] toolkit for its GPUs, both AMD and NVIDIA support the OpenCL [3] framework and Intel allows usage of standard programming tools and languages to program Intel MIC processor [4]. In addition there are also OpenACC [5] and OpenMP [6] standards that allow targeting hardware accelerators by expressing parallelism through compiler directives.

In this work Dynamic Kernel Scheduler (DKS) is presented which provides a slim software layer between host application and hardware accelerators. DKS allows to separate the accelerator and framework specific code from the host application and provides a simple interface, that can be implemented in the host application to offload tasks to the accelerator. DKS provides functions to handle communication and data transfer between host and device, and a library of functions written in CUDA, OpenCL and OpenMP that allow targeting different accelerators. The first version of DKS was integrated into OPAL (Object-oriented Parallel Accelerator Library). This DKS version uses CUDA kernels and OpenMP offload pragmas to run OPALs FFT based Poisson solver and Monte Carlo simulations for particle transport in a degrader on a GPU and Intel MIC. DKS was also used together with Minuit2 for parameter fitting, where χ^2 and max-log-likelihood functions were offloaded to the hardware accelerator.

In the literature there are several FFT Based Poisson solvers developed for GPUs using CUDA which use NVIDIA's cuFFT library [7, 8], there has also been research on using customized FFTs for asynchronous execution and mapping FFT based Poisson solvers to multi node systems [9, 10, 11]. Numerous studies [12, 13, 14, 15, 16, 17] have been carried out to show the potential of

GPUs and Intel Xeon Phi co-processors for Monte-Carlo simulations for proton and photon transport. These problems are ones of the most time consuming parts of the OPAL simulations, and previous research shows that they are good candidates for acceleration on the co-processors.

Many research projects try to focus on improving programmability of hardware accelerators. Apart from compiler directive based approaches there are a number of vendor supported libraries [18, 19], that allow to simplify offloading of specific tasks to accelerators. There has also been work on creating abstractions and providing software layers that would allow to express kernels [20, 21, 22] for hardware accelerators that can be translated to CUDA or OpenCL code that is run on the device.

The ability of DKS to have implementations using different frameworks and libraries, and switch between them from host applications allows not only to target hardware accelerators of different types and fine tune code to gain the maximum performance from each device, but also provides some software investment protection. In case some hardware architecture is no longer manufactured or some new architecture or development framework emerges only DKS needs to be updated.

The rest of the paper is structured as follows - Section 2 describes the concepts and architecture of DKS, in Section 3 the concepts of OPALs FFT based Poisson solver and Monte-Carlo type particle matter interaction simulations are described as well as DKS implementations of these functions, and benchmark results. Section 4 explains the DKS and MINUIT2 usage and results for parameter fitting using hardware acceleration, and Section 5 provides conclusions and future of the DKS.

2. Concept and Architecture of the Dynamic Kernel Scheduler (DKS)

2.1. Concept

Dynamic Kernel Scheduler (DKS) is a slim software layer between host application and hardware accelerator, as depicted in Figure 1. The aim of the DKS is to allow the creation of fast and fine tuned kernels using device specific frameworks such as CUDA, OpenCL, OpenACC and OpenMP. On top of that, DKS allows an easy use of these kernels in host application without providing any device or framework specific details. This approach facilitate the integration of different types of devices in the existing applications with minimal code changes and also makes the device and host code a lot more manageable.

The architecture of DKS can be split in three main parts:

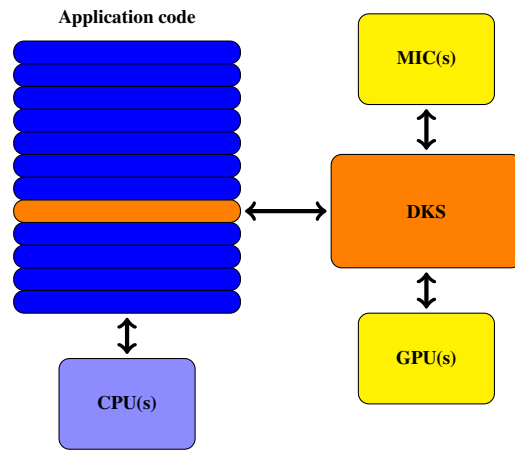


Figure 1: The Dynamic Kernel Scheduler concept

1. the first part provides communication functions that handle memory allocation and data transfer to and from the device. All the memory management is left up to the user, so the data transfers and memory allocation can be scheduled only when necessary. DKS also supports GPU streams so asynchronous data transfer and kernel execution can be implemented when possible.
2. the second part of DKS consists of function library, which contains algorithms written in CUDA, OpenCL and OpenMP to target different devices and DKS can switch between implementations based on the hardware that is available. Writing functions using multiple frameworks results in extra work, but this gives the opportunity to fine tune kernels for each device architecture for maximum performance, and target systems containing different types of devices. The different implementations of the code are always separated so the code is still easy to manage and if host application is targeted at a specific system, implementations that are not needed can be omitted.
3. the third part of DKS is the auto-tuning functionality and will be discussed in a forthcoming paper. The aim of auto-tuning is to select the appropriate implementation of the algorithm and change the launch parameters according to the devices that are available on the system in order to gain the maximum performance. The auto-tuning functionality relies on knowledge of device architecture and benchmark tests that can be run on the system before running the application.

```

//allocate memory on device and write data
void *mem_ptr;
mem_ptr = dks.allocateMemory<Complex_t>(DATA_SIZE, NULL);
dks.writeData<Complex_t>(mem_ptr, DATA_ARRAY, DATA_SIZE);

//execute FFT or IFFT
if (direction == 1)
    dks.callFFT(mem_ptr, DIMENSIONS, DIM_SIZE);
else
    dks.callIFFT(mem_ptr, DIMENSIONS, DIM_SIZE);

//read data and free memory
dks.readData<Complex_t>(mem_ptr, DATA_ARRAY, DATA_SIZE);
dks.freeMemory<Complex_t>(mem_ptr, DATA_SIZE);

```

Figure 2: Example of DKS usage for FFT

Figure 2 shows an example code of DKS usage inside host application to perform the Fast Fourier transform. The host application has a full control over the memory allocation and data transfer to the device, but there are no device specific details in the host code. DKS evaluates the calls made by host application and chooses the appropriate device to use and algorithm implementation to run the code on selected accelerator.

2.2. Architecture

Dynamic Kernel Scheduler is split into separate classes. Each class contains function implementations using different frameworks. Each of the DKS classes contains a constructor which handles the device management, memory management and data transfer for every development framework. The base part of the module can be extended to cover all the necessary algorithm specific functions. Base part of DKS receives all the calls from host application and decides which device specific implementation should be used to run the code on the device. Figure 3 shows the architecture of the first version of DKS, each of the base modules can be easily extended to include other algorithms and base part of DKS can be extended to include other development frameworks.

3. The Dynamic Kernel Scheduler used in Object-oriented Parallel Accelerator Library (OPAL)

OPAL (Object Oriented Particle Accelerator Library) is a parallel, open source C++ framework for general particle accelerator simulations including 3D space

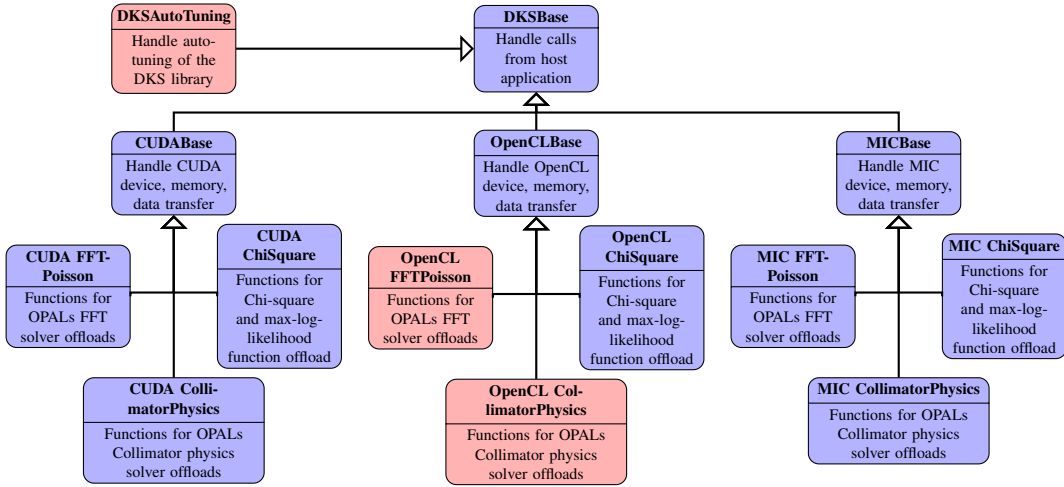


Figure 3: Architecture of the Dynamic Kernel Scheduler. The OpenCL implementation and the auto tuning framework both shown in red will be discussed in a subsequent publication.

charge, short range wake fields and particle matter interaction. OPAL is based on IPPL (Independent Parallel Particle Layer) which adds parallel capabilities. Main functions inherited from IPPL are structured rectangular grids, fields, parallel FFT and particles with the respective interpolation operators. Other features are, expression templates and massive parallelism (up to 65000 processors) which makes it possible to tackle the largest problems in the field.

3.1. FFT Based Particle-Mesh Solver

The Particle-Mesh (PM) solver is one of the oldest improvements over the Particle-Particle (PP) solver. Still one of the best references is the book by R.W. Hockney & J.W. Eastwood [23]. The PM solver introduces a discretisation of the rectangular computation domain $\Omega := [-L_x, L_x] \times [-L_y, L_y] \times [-L_z, L_z]$. This particle fitted grid is segmented into a regular mesh of $M_x \times M_y \times M_z$ grid points. The individual mesh sizes h_x, h_y and h_z are allowed to change independently over time, in order to assure a particle fitted grid.

The solution of Poisson’s equation is an essential component of any self-consistent electrostatic beam dynamics code that models the transport of intense charged particle beams in accelerators. If the bunch is small compared to the transverse size of the beam pipe, the conducting walls can be neglected. In such

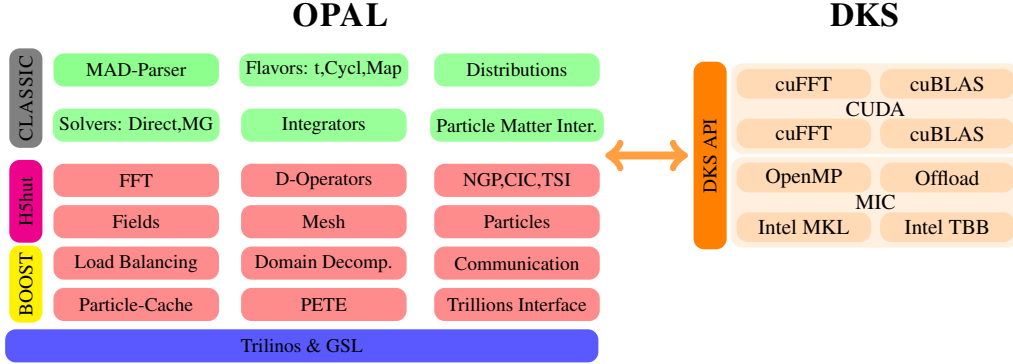


Figure 4: The OPAL software structure and connection to DKS

cases the Hockney method may be employed [23, 24, 25]. In that method, rather than computing N_p^2 point-to-point interactions (where N_p is the number of macro-particles), the potential is instead calculated on a grid of size $2^3 M_x M_y M_z$, where 3 spatial dimensions of the problem is assumed. Using the Hockney method, the calculation is performed using Fast Fourier Transform (FFT) techniques, with the computational effort scaling as $2^3 M_x M_y M_z (\log_2 2 M_x M_y M_z)^3$.

3.1.1. FFT-based convolutions

The solution of the Poisson equation,

$$\nabla^2 \phi = -\rho/\epsilon_0, \quad (1)$$

for the scalar potential, ϕ , due to a charge density, ρ , can be expressed as

$$\phi(x, y, z) = \int \int \int dx' dy' dz' \rho(x', y', z') G(x, x', y, y', z, z'), \quad (2)$$

where $G(x, x', y, y', z, z')$ is the Green function, subject to the appropriate boundary conditions, describing the contribution of a source charge at location (x', y', z') to the potential at an observation location (x, y, z) . For an isolated distribution of charge this reduces to

$$\phi(x, y, z) = \int \int \int dx' dy' dz' \rho(x', y', z') G(x - x', y - y', z - z'), \quad (3)$$

with

$$G(u, v, w) = \frac{1}{\sqrt{u^2 + v^2 + w^2}}. \quad (4)$$

A simple discretisation of Eq. (3) on a Cartesian grid with cell sizes h_x, h_y and h_z leads to,

$$\phi_{i,j,k} = h_x h_y h_z \sum_{i'=1}^{M_x} \sum_{j'=1}^{M_y} \sum_{k'=1}^{M_z} \rho_{i',j',k'} G_{i-i',j-j',k-k'}, \quad (5)$$

where $\rho_{i,j,k}$ and $G_{i-i',j-j',k-k'}$ denote the values of the charge density and the Green function, respectively, defined on the grid. The solution of Eq. (5) can be obtained using FFT based convolution, given by

$$\phi_{i,j,k} = h_x h_y h_z \text{FFT}^{-1}\{(\text{FFT}\{\rho_{i,j,k}\})(\text{FFT}\{G_{i,j,k}\})\} \quad (6)$$

where the notation has been introduced that $\text{FFT}\{.\}$ denotes a forward FFT in all 3 dimensions, and $\text{FFT}^{-1}\{.\}$ denotes a backward FFT in all 3 dimensions.

3.1.2. The DKS Implementation of the Poisson Solver

For use on NVIDIA GPUs FFT Poisson solver is implemented in DKS using CUDA. It uses NVIDIAAs provided cuFFT library to perform the FFT and separate kernels to calculate the Greens function and perform the multiplication on the GPU. CUDA streams are used to overlap the transfer of the ρ field to the GPU and calculation of the Greens function. The sequence diagram in figure 5 shows the steps executed for the FFT Poisson solver on the host and GPU. In case multiple host cores are sharing on GPU device CUDA inter-process communications are used to share the device memory between multiple MPI processes on the same node. For the FFT Poisson solver one of the MPI processes acts as a main process and initializes memory allocation and kernel execution on the device while other MPI processes only send and receive data to and from the GPU.

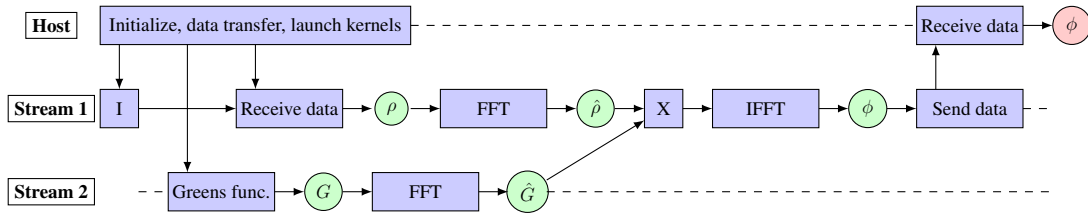


Figure 5: FFT-Poisson solver sequence diagram

3.1.3. Performance Results

To test the OPAL performance, we use a similar problem setup as reported in [26, 27]. The test system consists of host with two Intel Xeon e5-2609 v2

processors and a Nvidia Tesla K20. On the host, 8 CPU cores are available. First simulations were run using just the CPUs available on the host for calculations, but in the second case DKS is used to offload the FFT Poisson solver to the GPU.

Table 1: FFT Poisson Solver results

FFT size	DKS	Total time (s)	OPAL speedup	FFTPoisson time (s)	FFTPoisson speedup
64x64x32	no GPU	163.51		12.08	
		156.6	×1.04	4.09	×3
128x128x64	no GPU	219.29		103.53	
		132.47	×1.6	15.82	×6.5
256x256x128	no GPU	1143.39		933.08	
		318.01	×3.6	100.68	×9.3

Table 1 shows the results of these test runs for multiple problem sizes, which show that offloading FFT Poisson solver to GPU can provide a substantial speedup even when we have multiple CPU cores sharing one accelerator. The limiting factor for the performance of the FFT Poisson solver is the data transfer from the host side to the device, since data needs to be moved to and from GPU at every time step, for the largest problem size in the benchmark tests, this can take up to 55% of the total simulation time. Other limiting factor is the performance of the FFT transform. FFT is a memory bound algorithm and is able to reach only a fraction (about 10% was observed on our test system) of the device's peak performance, and for the Poisson solver FFT time is up to 80% of the calculation time spent on the GPU.

3.2. Particle Matter Interaction

One of the features of OPAL is the ability to perform Monte Carlo simulations of the particle beam interaction with matter. A fast charged particle moving through the material undergoes collisions with the atomic electrons and loses energy. In addition particles are also deflected from their original trajectory due to the Coulomb scattering with nuclei, as it is shown in figure 6. The energy loss in OPAL is calculated using the Bethe-Bloch formula and the change of particle trajectory is simulated using Multiple Coulomb Scattering and Single Rutherford Scattering [28, 29, 30]. At every time step when the particle beam is inside a material the following steps are executed:

- calculate the energy loss of the beam

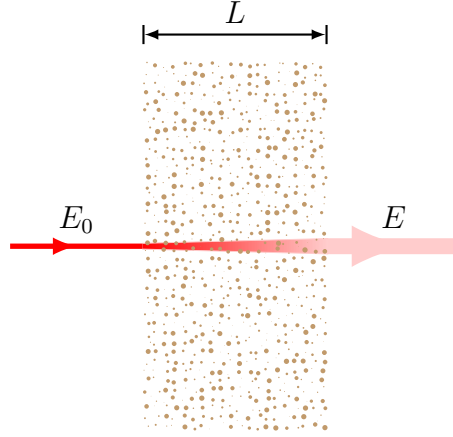


Figure 6: Particle matter interaction, final energy $E < E_0$ and larger momenta spread due to Coulomb scattering and the large angle Rutherford scattering.

- delete the particle if the particle's kinetic energy is smaller than a given threshold
- apply Coulomb & Rutherford scattering to the beam

3.2.1. The Energy Loss

The energy loss is calculated using the following Bethe-Bloch equation:

$$-dE/dx = \frac{Kz^2Z}{A\beta^2} \left[\frac{1}{2} \ln \frac{2m_e c^2 \beta^2 \gamma^2 T_{max}}{I^2} - \beta^2 \right], \quad (7)$$

where Z is the atomic number of absorber, A is the atomic mass of absorber, m_e is the electron mass, z is the charge number of the incident particle, $K = 4\pi N_A r_e^2 m_e c^2$, r_e is the classical electron radius, N_A is the Avogadro's number, I is the mean excitation energy. β and γ are kinematic variables. T_{max} is the maximum kinetic energy which can be imparted to a free electron in a single collision.

$$T_{max} = \frac{2m_e c^2 \beta^2 \gamma^2}{1 + 2\gamma m_e/M + (m_e/M)^2}, \quad (8)$$

where M is the incident particle mass.

For relatively thick absorbers such that the number of collisions is large, the energy loss distribution is shown to be Gaussian in form. For non-relativistic

heavy particles the spread σ_0 of the Gaussian distribution is calculated by:

$$\sigma_0^2 = 4\pi N_A r_e^2 m_e^2 c^4 \rho \frac{Z}{A} \Delta s, \quad (9)$$

where ρ is the density and s is the thickness of the material.

3.2.2. Coulomb scattering

The Coulomb scattering is treated as two independent events: the multiple Coulomb scattering and the large angle Rutherford scattering.

Using the distribution given in [31], the multiple- and single-scattering distributions can be written as:

$$P_M(\alpha)d\alpha = \frac{1}{\sqrt{\pi}} e^{-\alpha^2} d\alpha, \quad (10)$$

$$P_S(\alpha)d\alpha = \frac{1}{8 \ln(204Z^{-1/3})} \frac{d\alpha}{\alpha^3}, \quad (11)$$

where $\alpha = \frac{\theta}{(\Theta^2)^{1/2}} = \frac{\theta}{\sqrt{2}\theta_0}$. The transition point between multi and single scattering occurs for the angle $\theta = 2.5\sqrt{2}\theta_0 \approx 3.5\theta_0$, where value of θ_0 is the scattering angle from the Moliere's theory and is defined in equation 12.

$$\theta_0 = \frac{13.6MeV}{\beta cp} z \sqrt{\Delta s/X_0} [1 + 0.038 \ln(\Delta s/X_0)], \quad (12)$$

where p is the momentum, Δs is the step size, and X_0 is the radiation length.

To perform Monte Carlo simulation for the multiple Coulomb scattering two independent Gaussian random variables are created, with mean zero and variance one: z_1 and z_2 . The new position and momentum can then be calculated by:

$$x = x + \Delta s p_x + z_1 \Delta s \theta_0 / \sqrt{12} + z_2 \Delta s \theta_0 / 2, \quad (13)$$

$$p_x = p_x + z_2 \theta_0. \quad (14)$$

The values for the $y - p_y$ plane are calculated with the very same Monte-Carlo algorithm.

3.2.3. Large Angle Rutherford Scattering

Only small percentage of particles undergo large angle Rutherford scattering, this percentage is given by:

$$\chi_{single} < \frac{\int_{2.5}^{\infty} P_S(\alpha)d\alpha}{\int_0^{2.5} P_M(\alpha)d\alpha + \int_{2.5}^{\infty} P_S(\alpha)d\alpha} = 0.0047 \quad (15)$$

A random number ξ_1 between 0 and 1 is generated. If and only if this random number is smaller than χ_{single} the particle undergoes single Rutherford scattering. The value of χ_{single} does not change significantly for different materials, hence a fixed value of $\chi_{single} = 0.0047$ is used, in order to avoid unnecessary computation.

A second random variable ξ_2 between 0 and 1 is generated to calculate the angle, the particle rotates about.

The third and last random number ξ_3 determines the direction of the rotation:

$$\theta_{Ru} = \begin{cases} +2.5\sqrt{\frac{1}{\xi_2}}\sqrt{2}\theta_0 & \text{if } \xi_3 < 0.5 \\ -2.5\sqrt{\frac{1}{\xi_2}}\sqrt{2}\theta_0 & \text{if } \xi_3 > 0.5. \end{cases} \quad (16)$$

3.2.4. The DKS Implementation of the Particle Matter Interaction Model

For particle matter interaction DKS has CUDA and OpenMP implementations of all the algorithm steps described above, allowing computation of energy loss, Coulomb scattering and Rutherford scattering to be offloaded to the GPU or Intel MIC. On top of particle matter interaction DKS is also able to offload to the accelerators the transport of particles before and after the material using time integration scheme. The sequence diagram for the integration is shown in figure 7.

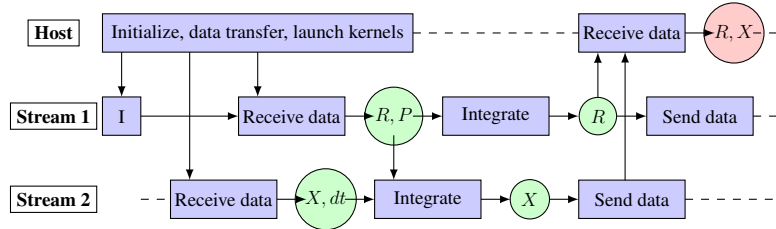


Figure 7: Integration sequence diagrams

To increase the performance the data transfer is minimized as much as possible, particles that are drifting before or after the degrader are kept on the device and are updated only when there is a some particles returning from material or there has been an MPI update to balance the workload between MPI processes. Pinned host memory and streams are used with the GPU version to increase the

date transfer speed and overlap the data transfer and kernel execution for the particle drift.

When particles enter the material they are also transferred to the accelerator only once. NVIDIA's cuRAND and Intel's MKL VSL libraries are used for random numbers, to get the necessary distributions for energy loss and scattering. Thrust library is used to sort and count the particles on the GPU, this is done in order to manage the particles that need to come out of the material and also to exclude the dead particles from Monte-Carlo simulations. Because of the high complexity of the algorithm CUDA version uses shared device memory for variable storage to reduce the register pressure of the kernels in order to achieve higher GPU occupancy. Structure of arrays data layout is used to store all the particles in order to allow Intel compiler to better vectorize the code for the Xeon Phi coprocessor. The sequence diagram of the degrader simulations on the CPU and device is shown in figure 8.

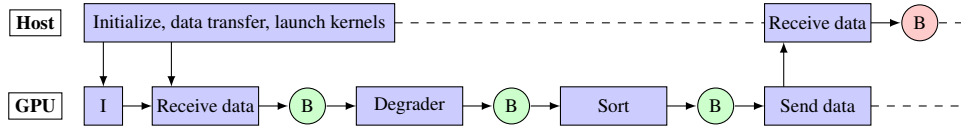


Figure 8: Degrader sequence diagrams, where B denotes particle bunch

3.2.5. Performance Results

To test the OPAL and DKS for the Monte Carlo simulations an example was run where particles are going through a $L = 1$ cm thick graphite slab, mimicking a degrader device used in proton therapy. Timings were obtained for the integration of the equation of motion, before and after the material and when the particles are moving through the material. The system setup is the same as was used for the FFT Based Particle-Mesh (PM) Solver benchmark.

Table 2 shows the benchmark results degrader and integration using various number of particles. The speedup of the particle transport through the material part of the algorithm is around $\times 140$ compared to the one core of the host processor, while the integration is able to achieve speedup of around $\times 20$ on the GPU. The Intel MIC on the other hand shows a speedup of $\times 40$ for the degrader and $\times 7$ for the integration compared to the host.

The limiting factor for GPU/MIC performance for the integration is the data movement, this operation requires data to be sent to the device and received from

Table 2: OPAL degrader results

Particles	DKS	Degrader time (s)	Degrader speedup	Integration time (s)	Integration speedup
10^5	no	20.30		3.46	
	GPU	0.28	×72	0.15	×23
	MIC	2.29	×8	0.89	×4
10^6	no	206.77		34.93	
	GPU	1.41	×146	1.83	×19
	MIC	5.38	×38	4.62	×7.5
10^7	no	2048.25		351.64	
	GPU	14.4	×142	17.21	×20

the device at every time step. In the case of GPU kernel execution can be completely overlapped with the data movement, so we are only limited by the memory bandwidth of our device.

The limiting factor for achieving even greater performance from GPU or Intel MIC for particle movement through the material is global memory access times, each execution of the kernel requires the load of position and momentum vectors as well as state of the random number generator for the thread, and, at the end of the kernel, position, momentum, random number state and possibly particle state needs to be updated. If there are any dead particles or particles that are coming out of the material these particles need to be removed from the bunch on the accelerator, this requires a sorting of the particles which also requires a lot of memory movement on the device and limits the performance.

4. Parameter Fitting with MINUIT2

MINUIT2 is a C++ library allowing a multi-parameter minimization of a user-defined function [32]. It is a re-implementation of the FORTRAN library MINUIT [33], a very popular minimization package used by high energy physicist. In addition to minimization algorithms, it contains methods for analyzing the solutions and estimate the parameter error correlation matrix. These combined capabilities are very difficult to find in other minimizers existing. Its drawback for inexperienced users is that the user-defined function needs to be implemented compiled and linked, which is a common practice in high energy physics but much less in the solid state physics community. Therefore, for the μ SR community, the MUSRFIT framework has been developed [34] which eases the analysis of muon spin

rotation, relaxation, and resonance (μ SR) experiments, since it allows the user to define all the relevant input parameters, functions, etc. in a scripting manner. We will describe the problem on the specific needs for μ SR, however the problem and the described solution is much more generic.

4.1. Problem description

In a time differential μ SR experiment [35], $\sim 100\%$ polarized positive muons (μ^+) are implanted in a solid sample and rapidly thermalize (~ 10 ps) without noticeable polarization loss. The spin evolution of the muon ensemble after implantation is then measured as a function of time. The evolution can be monitored by using the fact that the parity violating muon decay is highly anisotropic with the easily detectable positron emitted preferentially in the direction of the μ^+ spin at the moment of its decay. It takes the form

$$N^j(t) = N_0^j e^{-t/\tau_\mu} [1 + A^j(\mathbf{p}^j, t)] + N_{\text{bkg}}^j, \quad (17)$$

where the time is measured in discrete steps $t = n \cdot \Delta t$ [$n \in \mathbb{N}_0$, Δt the time resolution]. j indexing the positron detectors. The function $A^j(\mathbf{p}, t)$ describes the “physics” of the system under consideration. For details about the function $A^j(\mathbf{p}, t)$ the reader is referred to Ref. [35]. The muon lifetime is given by τ_μ , N_0 gives the scale of the positron count, and the constant N_{bkg}^j originates from uncorrelated background events. For a given positron histogram j the optimal parameter set

$$\mathbf{P}^j = \{N_0^j, N_{\text{bkg}}^j, \mathbf{p}^j\} \quad (18)$$

needs to be determined. Depending on the level of statistic of the positron histograms, this is either achieved with a χ^2 minimization:

$$\chi^2(\mathbf{P}) = \sum_j \sum_n \frac{[d_n^j - N^j(n \cdot \Delta t, \mathbf{P})]^2}{(d_{n,\text{err}}^j)^2}, \quad (19)$$

where d_n^j are the measured data points of j^{th} positron detector, the theory describing the data is given by Eq. (17), and $d_{n,\text{err}}^j$ the estimated error of d_n^j ($d_{n,\text{err}}^j = \sqrt{d_n^j}$ for the Poisson distributed positron histogram).

For data sets with rather limited statistics Eq. (19) is not leading to satisfactory results. In this case the log-likelihood function

$$\mathcal{L} = 2 \cdot \sum_j \sum_n \begin{cases} [N^j(n \cdot \Delta t, \mathbf{P}) - d_n^j] + d_n^j \log \left[\frac{d_n^j}{N^j(n \cdot \Delta t, \mathbf{P})} \right], & d_n^j > 0 \\ [N^j(n \cdot \Delta t, \mathbf{P}) - d_n^j] & d_n^j \leq 0 \end{cases} \quad (20)$$

should be maximized, leading to much better estimates of \mathbf{P} .

In recent years changes in the detector technology allow higher time resolution (smaller detectable Δt) at the expense of a higher detector fragmentation (more positron counters). This is leading to much larger data sets, and henceforth the minimization/maximization times are exploding. This is especially true if a parameter error estimate is needed which is going beyond the simple Hessian approach.

The MINUIT2 library is almost perfectly suited to tackle the above problem. The user needs to implement Eqs. (19) and/or (20) on the accelerator(s), whereas the minimization process is executed on the host. The main and most time consuming part in the calculation is given by Eqs. (19) and (20). The only data transfer needed between the host and the accelerator is given by the small parameter set \mathbf{P} which should not lead to a bottleneck in the all over computation time.

4.1.1. The DKS Implementation

For parameter fitting with Minuit2 DKS is used to offload the χ^2 , max-log-likelihood and the user defined function calculations to the GPU. The calculated value is passed to Minuit2 which varies the parameter set and returns the new parameters. Data transfer from host to device is minimal, measurement data are transferred to the GPU only once at the beginning of the calculations and at every step only the parameter array is transferred to device and only the χ^2 or max-log-likelihood value is returned by the device. CUDA and OpenCL are implemented to support various hardware accelerators.

4.1.2. Performance Results

Parameter fitting tests with Minuit2 and DKS were performed on the same machine as OPAL tests, host code used 8 CPU cores and parallelization was done using OpenMP, while the device code was run on Nvidia Kepler 20k using CUDA or OpenCL kernels. Results for offloading χ^2 and max-log-likelihood functions are shown in the table 3, since there is almost no data transfer involved in the program and the problem is very easy to parallelize. The time to solution on

the device is about 300 times faster for χ^2 and about 150 times faster for max-log-likelihood functions than currently used OpenMP implementation for the host CPUs. For the results presented in Tab. 3, $A^j(\mathbf{p}, t)$ was chosen as

$$A^j(\mathbf{p}, t) = A_0^j \exp \left[-\frac{1}{2}(\sigma t)^2 \right] \cos(\gamma_\mu B t + \phi^j), \quad (21)$$

with $j = 1 \dots 16$, A_0^j are the asymmetries of each positron detector, σ the depolarization rate of the muon spin ensemble, γ_μ the gyromagnetic ratio of the muon, B the magnetic induction at the muon stopping site, t the time [see Eq.(17)], and ϕ^j the phase of the initial muon spin in respect to the positron detector. Eq.(21) is a typical muon polarization function to determine the magnetic shift of a para-/diamagnetic material (see Ref. [35]). For the given number of positron detectors 66 fitting parameters needed to be determined [see Eqs.(17), (21)].

Table 3: Minuit2 parameter fitting with χ^2 and max-log-likelihood (MLE) function running on the GPU. The given time is for the execution of the `migrad` command of Minuit2 [32].

Data Set Size	DKS	χ^2 (s)	Speedup	MLE (s)	Speedup
~1,300,000	no	157.077		446.444	
	yes (CUDA)	0.55012	×285	2.75018	×162
	yes (OpenCL)	0.72	×218	-	
~1,700,000	no	264.279		664.893	
	yes (CUDA)	0.863937	×306	4.16143	×160
	yes (OpenCL)	1.17741	×224	-	
~2,200,000	no	392.727		741.114	
	yes (CUDA)	1.32307	×296	5.2768	×140
	yes (OpenCL)	1.80757	×217	-	
~3,300,000	no	859.339		1101.62	
	yes (CUDA)	2.52918	×339	7.60934	×144
	yes (OpenCL)	3.61519	×237	-	

5. Conclusion and Outlook

In this paper we presented the first version of Dynamic Kernel Scheduler which provides a software layer between host application and hardware accelerators. This allows to create a fine tuned code for different hardware accelerators using different frameworks and easily integrate it into existing host applications.

DKS was integrated into OPAL to offload FFT based Poisson solver and Monte-Carlo simulations for particle matter interaction to GPU and Intel MIC using either CUDA or OpenMP. DKS was also used together with Minuit2 for parameter fitting where χ^2 and *max - log - likelihood* function calculations were offloaded to GPU using CUDA or OpenCL. The results of this work show that DKS can be used to substantially speed up existing host applications with minimal additions and changes to host code. Separating the device specific code in a different layer allows managing and fine tuning the code more easily and it also keeps the host application a lot more portable since all the device and framework specific details are handled by DKS.

6. References

References

- [1] Top500 supercomputers, <http://www.top500.org/lists/2015/06/>.
- [2] NVIDIA CUDA Zone, <https://developer.nvidia.com/cuda-zone>.
- [3] Khronos Group, OpenCL, <https://www.khronos.org/opencl/>.
- [4] Intel Xeon Phi coprocessor, <https://software.intel.com/en-us/mic-developer>.
- [5] OpenACC, <http://www.openacc.org/>.
- [6] OpenMP, <http://openmp.org/wp/openmp-specifications/>.
- [7] V. K. Decyk, T. V. Singh, Adaptable Particle-in-Cell algorithms for graphical processing units, *Computer Physics Communications* 182 (3) (2011) 641–648.
- [8] D. Rossinelli, M. Bergdorf, G.-H. Cottet, P. Koumoutsakos, GPU accelerated simulations of bluff body flows using vortex particle methods, *Journal of Computational Physics* 229 (9) (2010) 3316–3333.
- [9] N. Dugan, L. Genovese, S. Goedecker, A customized 3D GPU Poisson solver for free boundary conditions, *Computer Physics Communications* 184 (8) (2013) 1815–1820.
- [10] J. Wu, J. JaJa, High performance FFT based poisson solver on a CPU-GPU heterogeneous platform, *Proceedings - IEEE 27th International Parallel and Distributed Processing Symposium, IPDPS 2013* (2013) 115–125.

- [11] J. Wu, J. JaJa, Optimized FFT computations on heterogeneous platforms with application to the Poisson equation, *Journal of Parallel and Distributed Computing* 74 (8) (2014) 2745–2756.
- [12] T. H. Osiecki, M.-y. Tsai, A. E. Gattiker, D. a. Jamsek, S. R. Nassif, W. E. Speight, C. C. Sze, Hardware Acceleration of an Efficient and Accurate Proton Therapy Monte Carlo, *Procedia Computer Science* 18 (2013) 2241–2250.
- [13] X. Jia, T. Pawlicki, K. T. Murphy, A. J. Mundt, Proton therapy dose calculations on GPU: advances and challenges, *Translational Cancer Research* 1 (3) (2012) 207–216.
- [14] X. Jia, X. Gu, Y. J. Graves, M. Folkerts, S. B. Jiang, GPU-based fast Monte Carlo simulation for radiotherapy dose calculation (2011) 18.
- [15] T. Liu, X. Xu, C. Carothers, Comparison of two accelerators for Monte Carlo radiation transport calculations, Nvidia Tesla M2090 GPU and Intel Xeon Phi 5110p coprocessor: A case study for X-ray CT imaging dose calculation, *Annals of Nuclear Energy* 82 (2015) 230–239.
- [16] X. G. Xu, T. Liu, L. Su, X. Du, M. Riblett, W. Ji, D. Gu, C. D. Carothers, M. S. Shephard, F. B. Brown, M. K. Kalra, B. Liu, ARCHER, a new Monte Carlo software tool for emerging heterogeneous computing environments, *Annals of Nuclear Energy* 82 (2015) 2–9.
- [17] J. Tickner, Monte Carlo simulation of X-ray and gamma-ray photon transport on a graphics-processing unit, *Computer Physics Communications* 181 (11) (2010) 1821–1832.
- [18] GPU Accelerated Libraries, <https://developer.nvidia.com/gpu-accelerated-libraries>.
- [19] Intel Math Kernel Library (Intel MKL), <https://software.intel.com/en-us/articles/intel-mkl-on-the-intel-xeon-phi-coprocessors>.
- [20] M. Bourgoïn, E. Chailloux, J. L. Lamotte, Efficient abstractions for GPGPU programming, *International Journal of Parallel Programming* 42 (4) (2014) 583–600.

- [21] J. Svensson, K. Claessen, M. Sheeran, GPGPU kernel implementation and refinement using Obsidian, *Procedia Computer Science* 1 (1) (2010) 2065–2074.
- [22] M. Viñas, B. B. Fraguera, Z. Bozkus, D. Andrade, Improving OpenCL Programmability with the Heterogeneous Programming Library, *Procedia Computer Science* 51 (2015) 110–119.
- [23] R. Hockney, *Methods in computational physics*, Alder, B (1970) 136–211.
- [24] J. W. Eastwood, D. R. K. Brownrigg, *J. comp. phys.*, 32, 24-38, *J. Comp. Phys.*, 32, 24-38.
- [25] R. Hockney, J. Eastwood, *Computer Simulation using Particles*, Adam Hilger, 1988.
- [26] e. a. Y. Bi, A. Adelman, *Phys. rev. stab* **14**(5) 054402, *Phys. Rev. STAB* **14**(5) 054402.
- [27] e. a. J. Yang, A. Adelman, *Phys. rev. stab* **13**(6) 064201, *Phys. Rev. STAB* **13**(6) 064201.
- [28] Stopping powers and ranges for protons and alpha particles, ICRU Report 49.
- [29] K. O. et al, Particle data group, *Chin. Phys. C*, 38, 090001.
- [30] W. R. Leo, *Techniques for nuclear and particle physics experiments*, 2nd Edition, Springer-Verlag, Berlin Heidelberg New York, 1994.
- [31] J. D. Jackson, *Classical Electrodynamics*, 3rd Edition, John Wiley & Sons, New York, 1998.
- [32] L. Moneta, M. Winkler, A. Zsenei, P. Mato-Vila, M. Hatlo, F. James, Developments of mathematical software libraries for the lhc experiments, *IEEE Transactions on Nuclear Science* 52 (2005) 2818–2822.
- [33] C. Group, *Minuit users guide*, Program Library D506, CERN.
- [34] A. Suter, B. Wojek, *Musrfit: a free platform-independent framework for μ SR data analysis*, *Physics Procedia* 30 (2012) 69–73.
- [35] A. Youanc, P. D. de Réotier, *Muon spin rotation, relaxation and resonance*, Oxford University Press, Oxford, 2011.